

# Hydroacoustic Travel Time Variations as a Proxy for Passive Deep-Ocean Thermometry

Pieter Smets<sup>1</sup>, Cornelis Weemstra<sup>1</sup>, and Láslo Evers<sup>2</sup>

<sup>1</sup>Delft University of Technology

<sup>2</sup>Royal Netherlands Meteorological Institute

November 23, 2022

## Abstract

We report on the extraction of deep ocean travel time variations from time-lapse cross-correlations between a hydrophone station and a three-component broadband seismometer. The signals we cross-correlate in this study result from repeated activity by the Monowai seamount, one of the most active submarine volcanoes of the Tonga-Kermadec ridge. In particular, we introduce a specific workflow to exploit repetitive hydroacoustic underwater source activity, which we detail to such extent that it serves as an example (or “cookbook”). For this reason, we have made the source code publicly available. The workflow proposed in this study (i) overcomes differences in instrument sensitivity and sample rates, (ii) involves the selection of eligible cross-correlations based on a source activity criterium as well as slowness analysis, and (iii) extracts the travel time variations in distinct frequency bands. In our case, the two frequency bands are 3-6 Hz and 6-12 Hz. We find that the estimated travel time variations in both frequency bands consist of a complex periodic pattern superimposed on a distinct long-term linear trend. This long-term linear trend is decreasing, which we attribute to increasing water temperatures along the propagation path of the hydroacoustic signals.

# Hydroacoustic Travel Time Variations as a Proxy for Passive Deep-Ocean Thermometry



Pieter Smets\* (1,2), Kees Weemstra (1, 2), Láslo Evers (2, 1)

1. Royal Netherlands Meteorological Institute (KNMI), 2: Delft University of Technology (TU Delft);

\*presenting author



PRESENTED AT:



## SUMMARY

We extract deep ocean travel time variations from time-lapse cross-correlations between a hydrophone station and a three-component broadband seismometer.

The signals result from repeated activity by the Monowai seamount, one of the most active submarine volcanoes of the Tonga-Kermadec ridge.

The introduced workflow: (i) overcomes differences in instrument sensitivity and sample rates, (ii) involves the selection of eligible cross-correlations based on a source activity criterium as well as slowness analysis, and (iii) extracts the travel time variations in distinct frequency bands.

Source code and examples are publicly available (<https://gitlab.com/psmsmets/xcorr>)

# INSTRUMENTATION

Hydrophone triplet **H03S**, part of the International Monitoring System for the verification of the Comprehensive Nuclear-Test-Ban Treaty (CTBT), sampling at 250 Hz.

Three-component Streckeisen seismometer at station **RAR** with location code *10*, sampling at 40 Hz. We only use seismic waves in the vertical plane (vertical and radial components only).

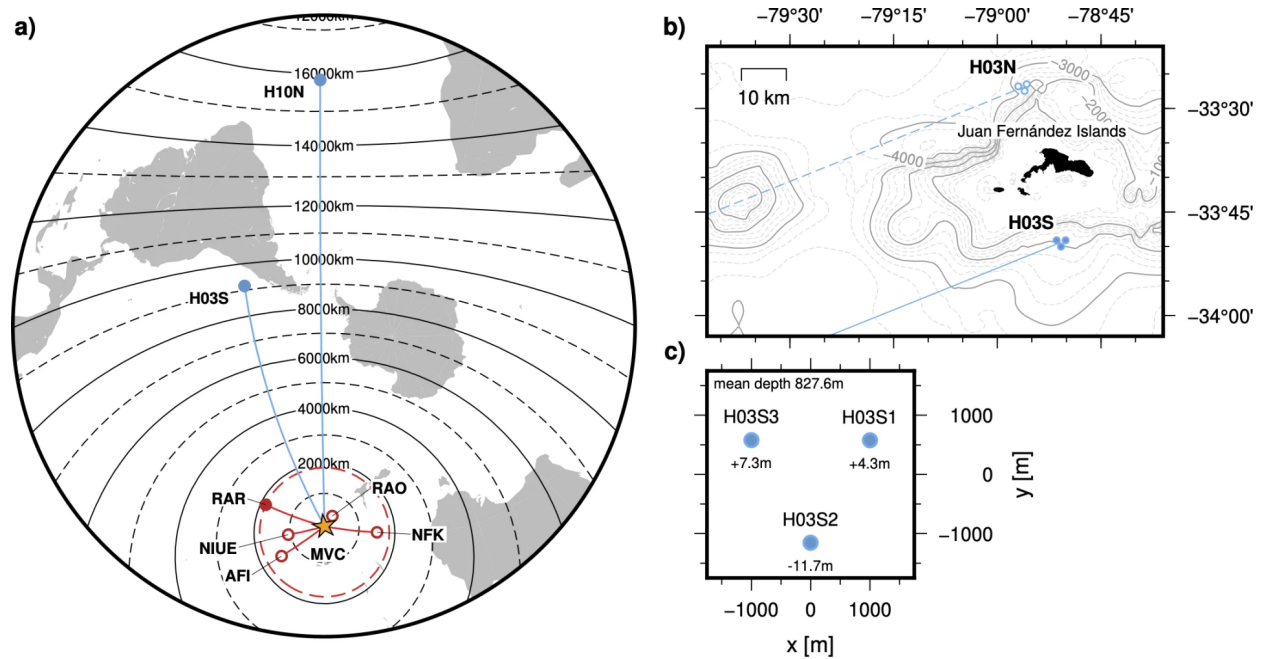


**Figure:** (a) Map of the Monowai volcanic centre (MVC, yellow star), broadband seismic stations within a 2000 km radius (red circles) and hydroacoustics triplets H03S and H10N (blue circles). Solid circles indicate a direct line of sight through the SOFAR channel. (b) Map depicting the hydrophone triplets H03N (obstructed line of sight) and H03S (direct line of sight) near the Juan Fernández Islands, Chile. (c) Hydrophone triplet layout in local coordinates; vertical deviation from mean depth is indicated for the individual elements.

# CROSS-CORRELATION FUNCTIONS (CCFS)

Distant hydroacoustic observations Monowai are cross-correlated with “closer” seismic T-phase observations.

A pre-processing workflow is proposed that retains phase and spectral information for the cross-correlation analysis. We minimally pre-process waveforms in the sense that CCFs can be filtered later in the workflow retaining as much spectral information as possible.

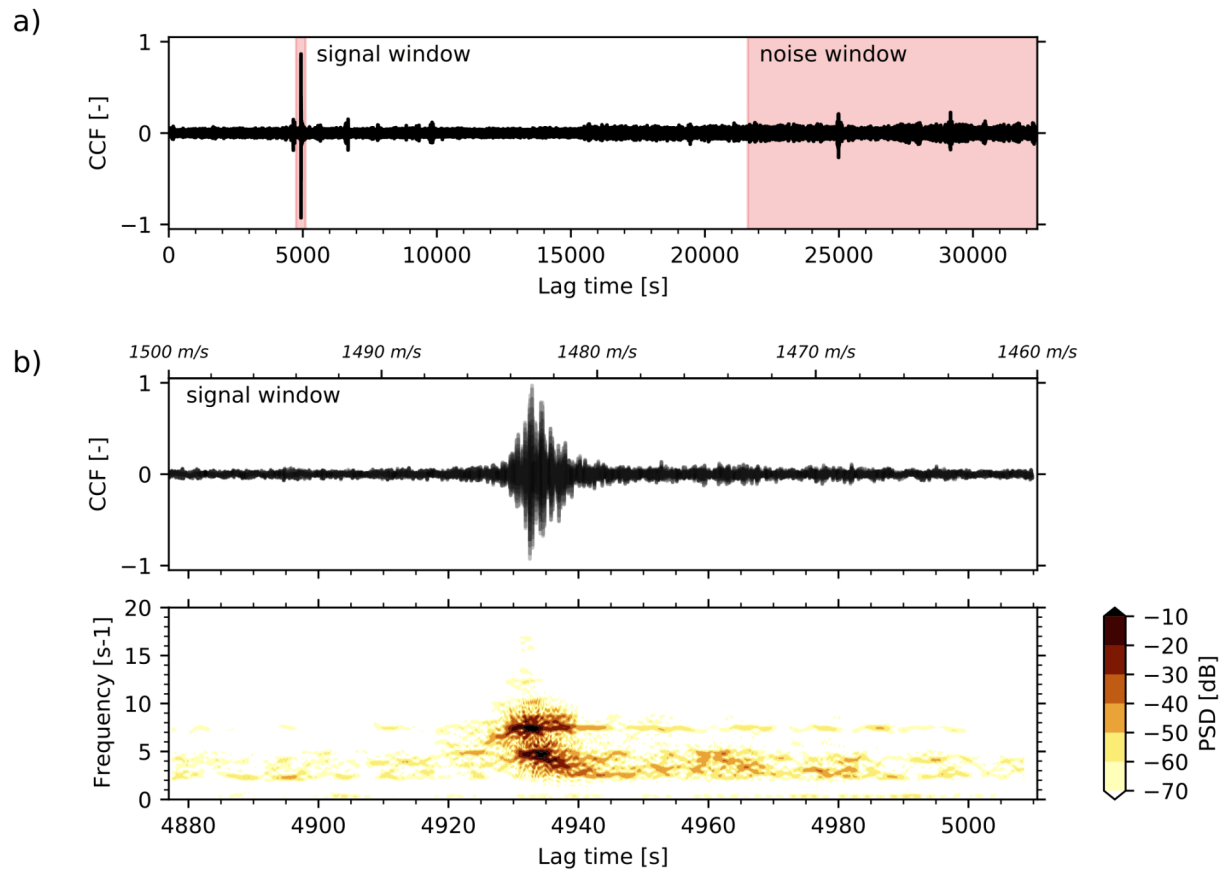


**Figure:** (a) CCF between *IM.H03S1..EDH* and *IU.RAR.10.BHZ* for 15 January 2015 (unbiased, demeaned, high-pass filtered with a zero-phase 2nd order Butterworth filter with a 3 Hz corner frequency, and normalized). (b) Zoom-in on the signal window (top) and the corresponding spectrogram (power spectral density) for 2.5 s subwindows with a padding factor of 4 (bottom). Indicated velocities correspond to the time lag and the relative distance between the two receivers.

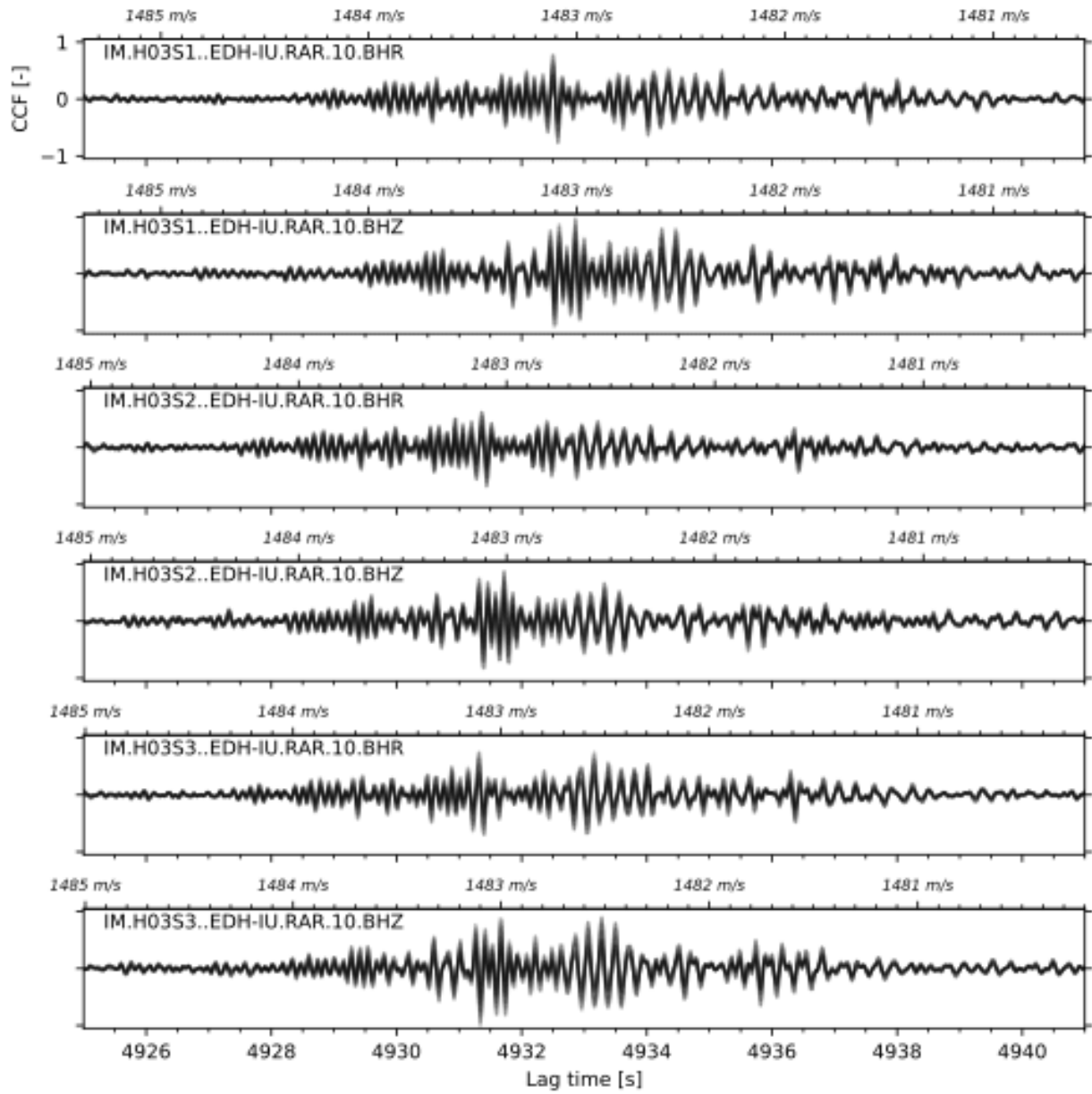


**Figure:** CCFs between RAR and H03S for 15 January 2015 (unbiased, demeaned, high-pass filtered with a zero-phase 2nd order Butterworth filter with a 3 Hz corner frequency, and normalized). All 8 CCFs with 3 h increments corresponding to the same day are plotted on top of each other. Indicated velocities correspond to time lag and the relative distance for the given receiver pair.

# SYSTEMATIC CCF SELECTION

We propose an automatic selection criterion to account for non-continuous and spurious MVC activity. CCFs eligible for time-lapse analysis are selected based on: (i) source activity and (ii) source directionality.

(i) **Source activity** is quantified by the signal-to-noise ratio (S/N) of the CCFs. Eligible source activity corresponds to coincidence triggered periods with an S/N threshold of 10 and a minimum duration of one day.

- **signal window:** time lags proportional to the velocity range for SOFAR channel propagation (1450 to 1520 m s<sup>-1</sup>) along with the relative distance between the two receivers and the source (7,308.1 km).
- **noise window:** 6 to 9 h posterior time lags with the same sign as the signal window.

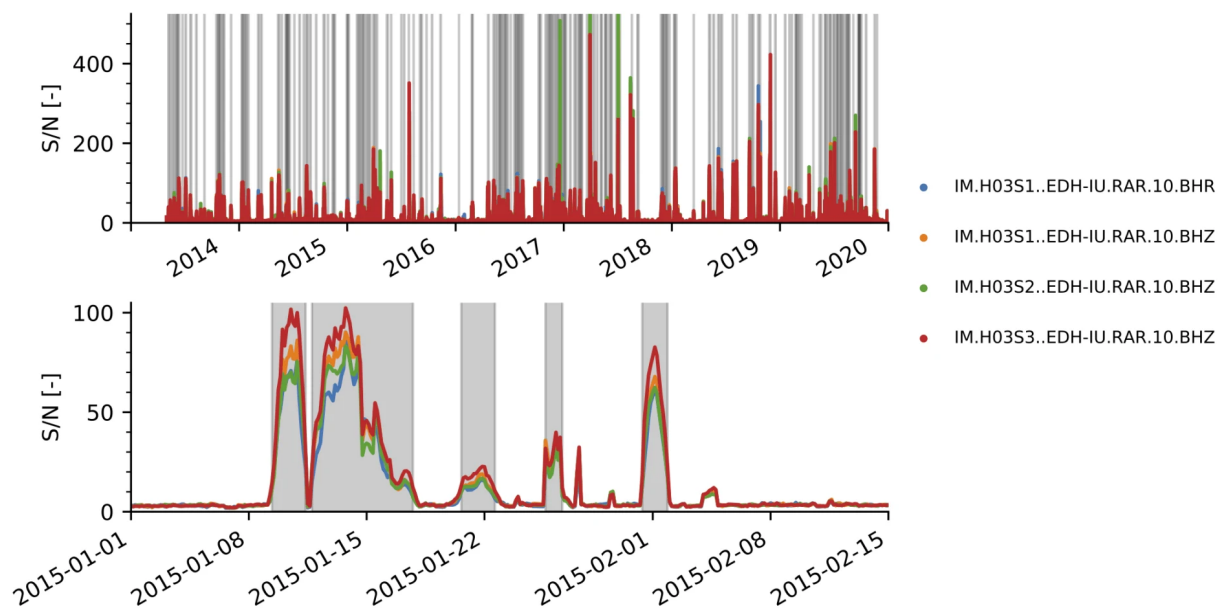


**Figure:** Signal-to-noise ratio for 2014-2020 (top) and a zoom-in on an active period (bottom). Eligible source activity is indicated in grey.

(ii) **Source directionality** is estimated assuming a plane wave traversing the hydrophone triplet and is applied to the CCFs of the three acoustic channels with the vertical seismic component.

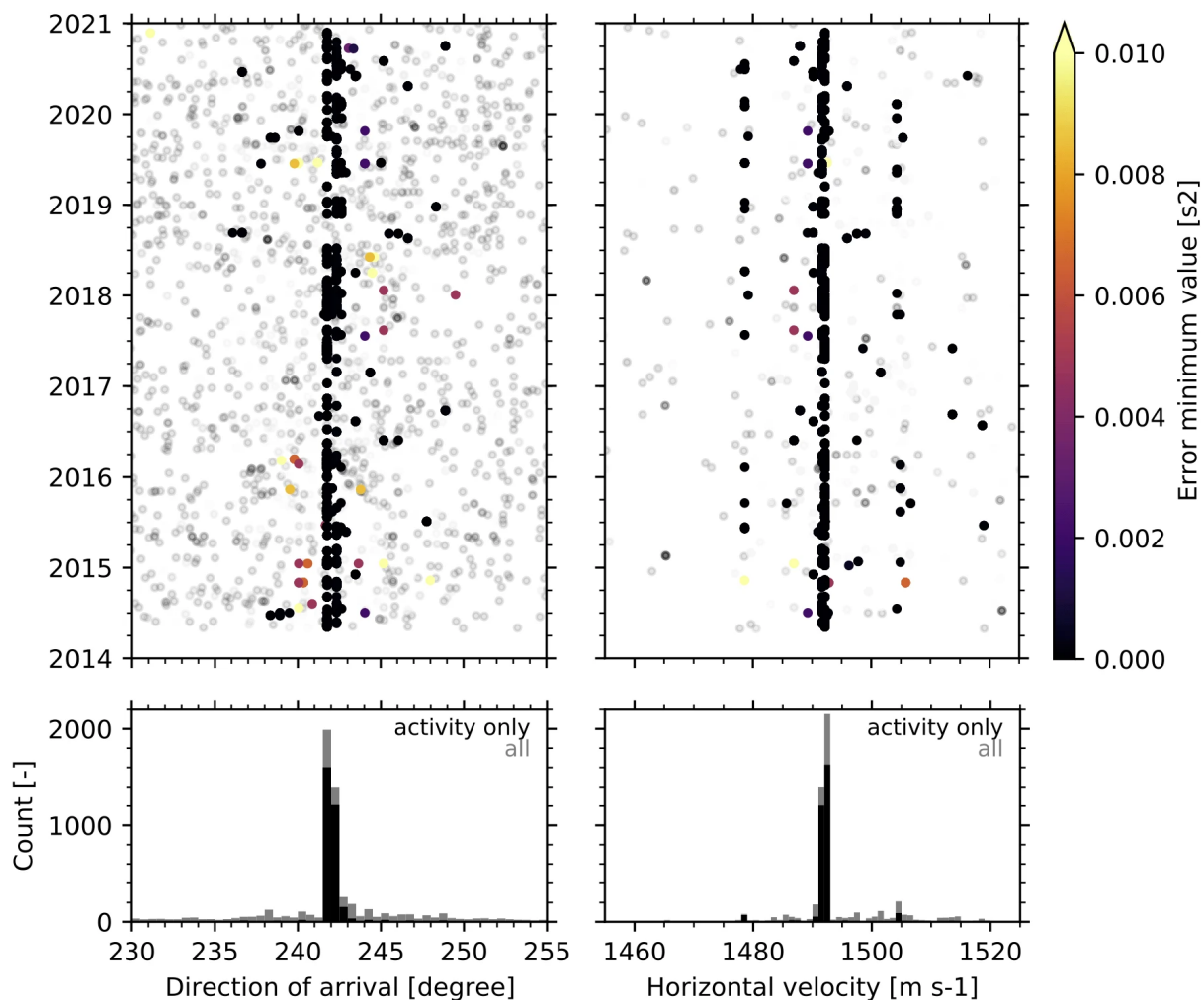


**Figure:** Estimated plane wave characteristics as a function of time using the CCF signal windows. Coloured circles in the top row correspond to S/N triggered activity only whereas light-grey circles correspond to the non-triggered CCFs.

# TRAVEL TIME VARIATIONS

We extract frequency-dependent travel time variations from time-lapse cross-correlations for the eligible periods.

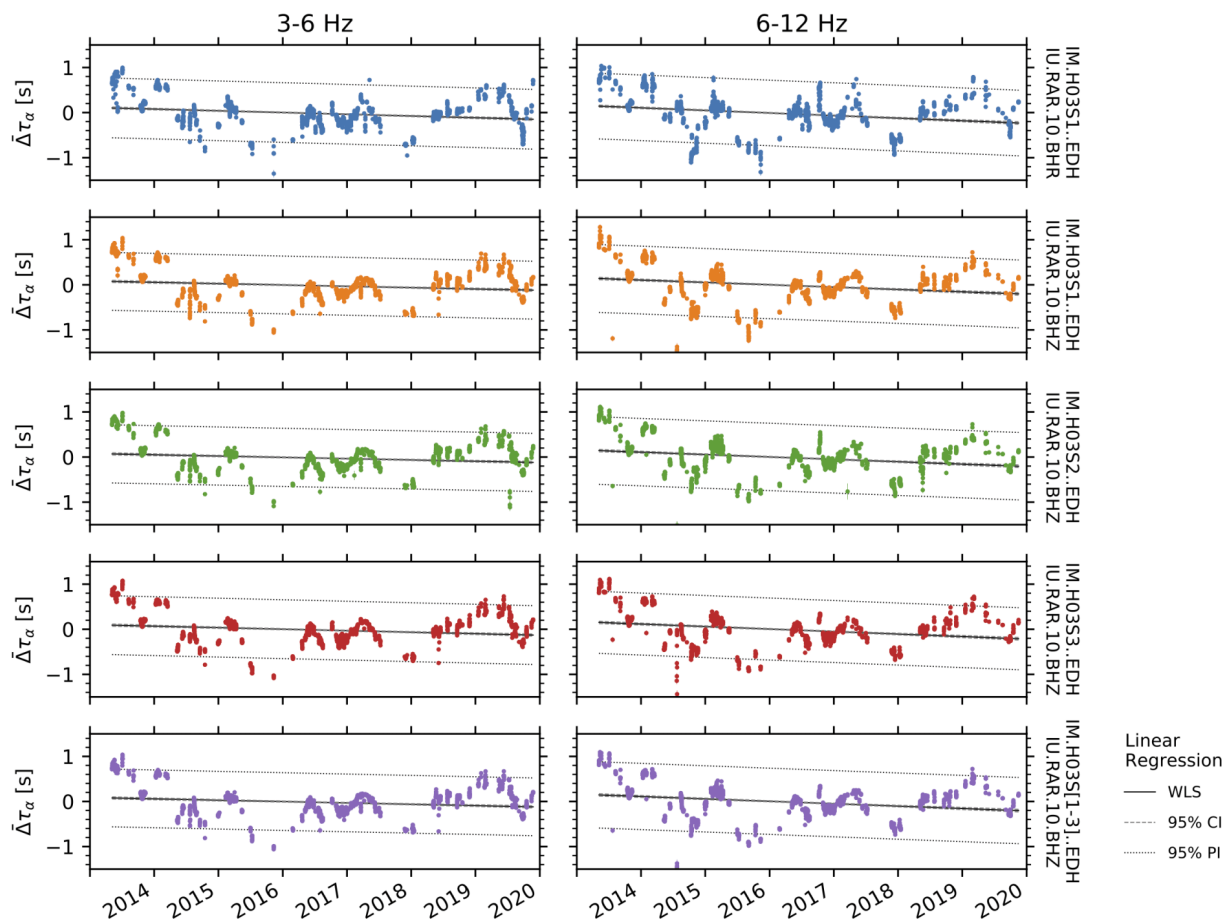


**Figure:** Trimmed weighted mean lag time variation with the 95% confidence interval as a function of time. Trimmed subsets per time step are confined by the 0.02 and 0.98 percentiles. Sloped horizontal lines are the corresponding linear regressions (solid red line) with the 95% confidence interval (dashed blue lines, percentile distribution) and the 95% prediction interval (dashed green lines, parametric estimate) obtained from 20,000 bootstrap estimations.

We find that the estimated travel time variations in both frequency bands consist of a complex periodic pattern superimposed on a distinct long-term linear trend. This long-term linear trend is decreasing, which we attribute to increasing water temperatures along the propagation path of the hydroacoustic signals.

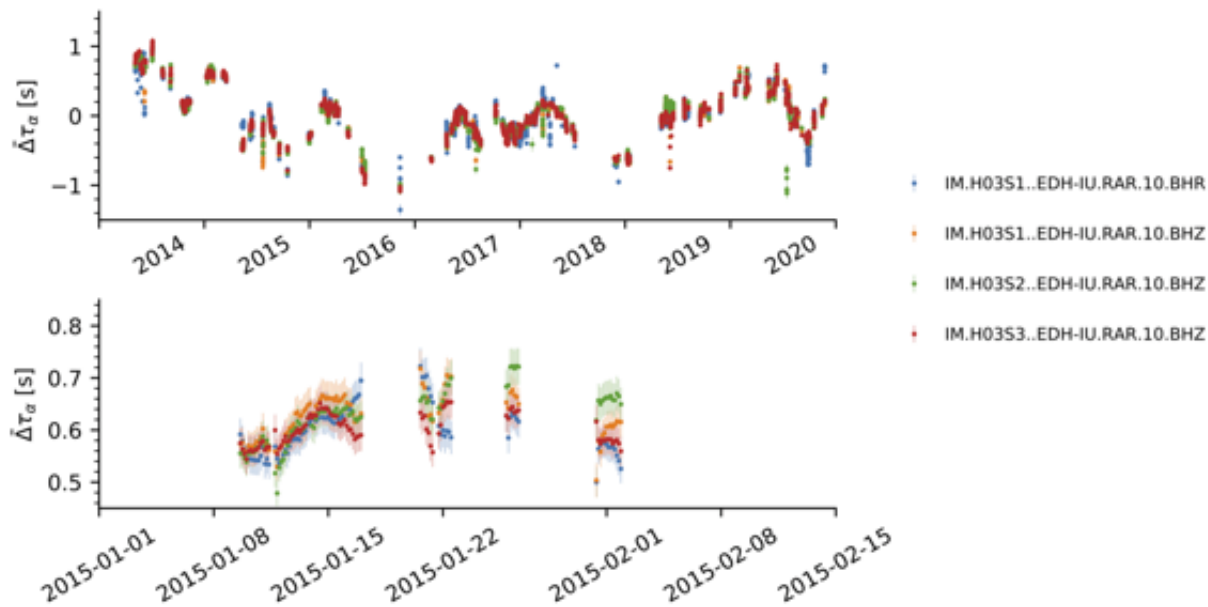


Figure: Trimmed weighted mean lag time variation with the 95% confidence interval as a function of time for the 3-6Hz octave.

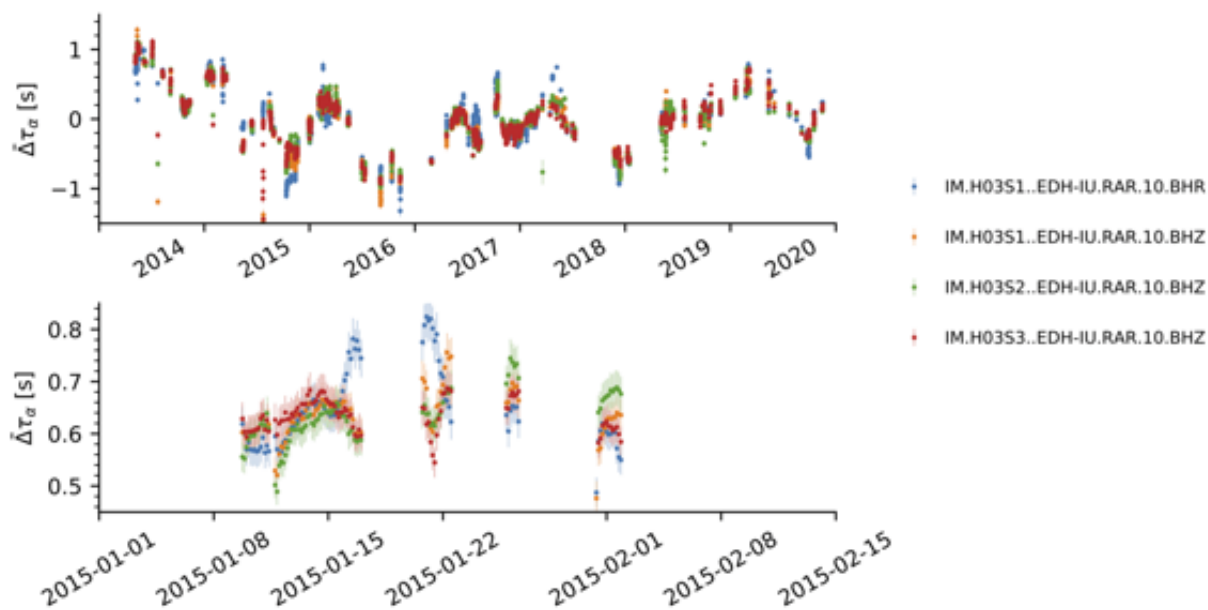
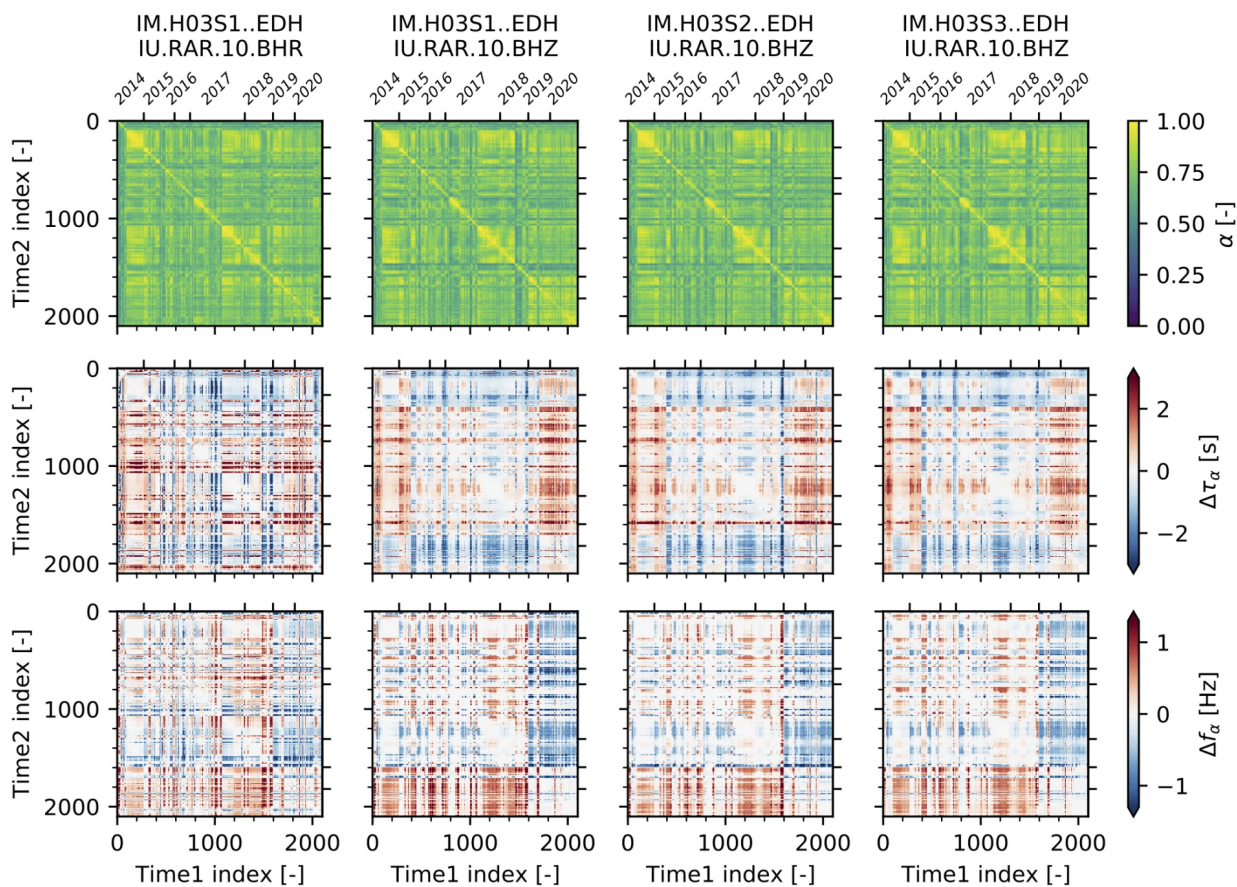


Figure: Trimmed weighted mean lag time variation with the 95% confidence interval as a function of time for the 6-12Hz octave.

# TIME-LAPSE CROSS-CORRELATIONS

We apply time-lapse cross-correlation analysis to the eligible CCFs spectrograms in two discrete frequency bands of 3-6 Hz and 6-12 Hz.



**Figure:** Time-lapse results for the 3–6 Hz octave band, filtered for spurious time combinations.

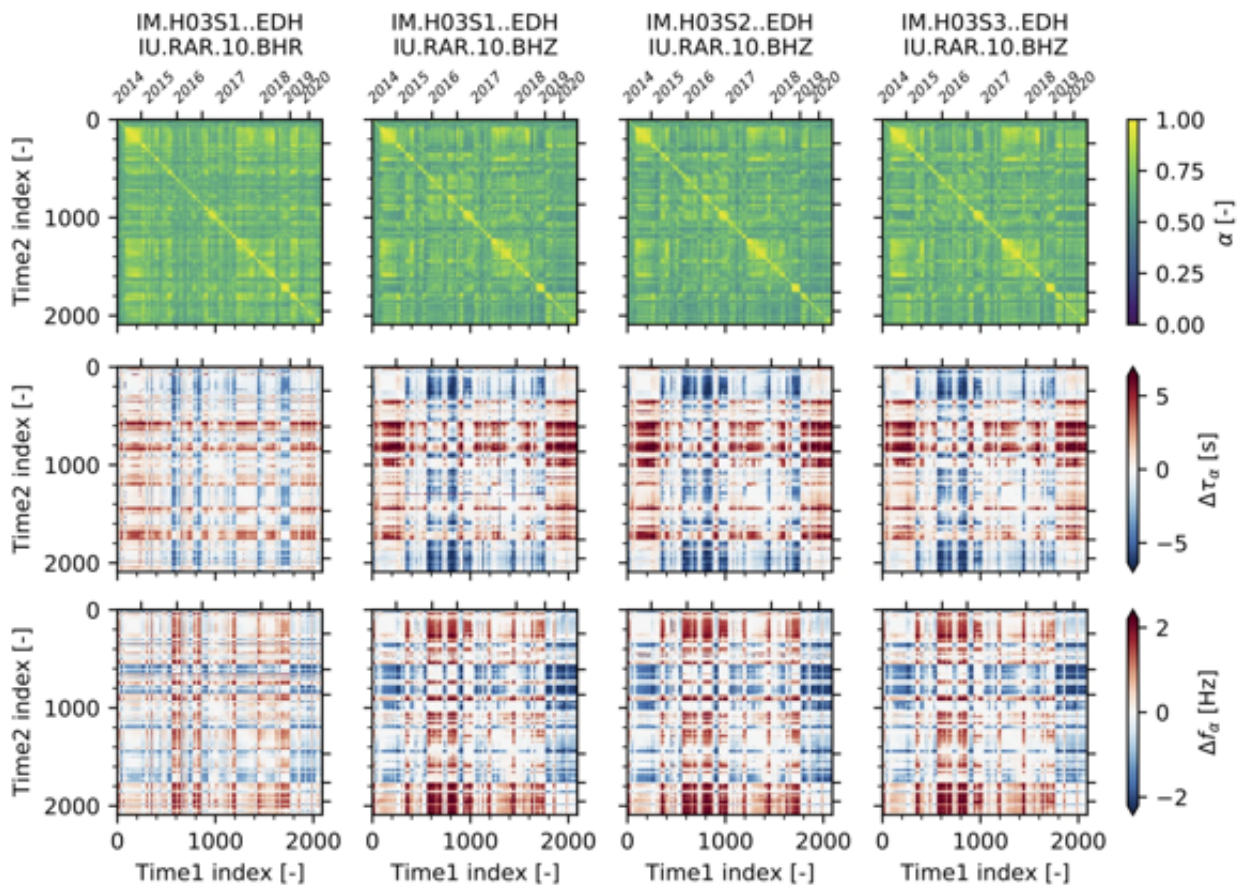


Figure: Time-lapse results for the 6–12 Hz octave band, filtered for spurious time combinations.

## AUTHOR INFORMATION

The CTBTO station operators are thanked for the high-quality data and products. Hydroacoustic data can be requested at the CTBTO International DataCenter (IDC) in Vienna, via the virtual Data Exploration Center. Broadband seismic data and hydroacoustic data of H10 since 2015 are openly available on IRIS (<https://iris.edu>).

Source code is available on GitLab (<https://gitlab.com/psmsmets/xcorr>) containing the Python3 module and examples. The code is build around ObsPy (<https://obspy.org>), NumPy (<https://numpy.org>), SciPy (<https://scipy.org>), xarray (<http://xarray.pydata.org>), pandas (<http://pandas.pydata.org>) and Dask (<https://dask.org>).

Figures were prepared using the Generic Mapping Tools, Matplotlib (<https://matplotlib.org>), and Seaborn (<http://seaborn.pydata.org>).

Pieter S. M. Smets and Láslo G. Evers's contributions are funded through a VIDI project from the Netherlands Organization for Scientific Research (NWO), Project 864.14.005.

The manuscript is in preparation for submission.

## ABSTRACT

We report on the extraction of deep ocean travel time variations from time-lapse cross-correlations between a hydrophone station and a three-component broadband seismometer. The signals we cross-correlate in this study result from repeated activity by the Monowai seamount, one of the most active submarine volcanoes of the Tonga-Kermadec ridge. In particular, we introduce a specific workflow to exploit repetitive hydroacoustic underwater source activity, which we detail to such extent that it serves as an example (or "cookbook"). For this reason, we have made the source code publicly available. The workflow proposed in this study (i) overcomes differences in instrument sensitivity and sample rates, (ii) involves the selection of eligible cross-correlations based on a source activity criterium as well as slowness analysis, and (iii) extracts the travel time variations in distinct frequency bands. In our case, the two frequency bands are 3-6 Hz and 6-12 Hz. We find that the estimated travel time variations in both frequency bands consist of a complex periodic pattern superimposed on a distinct long-term linear trend. This long-term linear trend is decreasing, which we attribute to increasing water temperatures along the propagation path of the hydroacoustic signals.

## REFERENCES

- Bendat, J. S., & Piersol, A. G. (1987). *Random Data: Analysis and Measurement Procedures* (Fourth ed.). Wiley. doi: 10.2307/2289430
- Dahlman, O., Mykkeltveit, S., & Haak, H. (2009a). Monitoring Technologies. In *Nuclear test ban* (pp. 25–58). Dordrecht: Springer Netherlands. doi: 10.1007/978-1-4020-6885-0\_2
- Metz, D., Watts, A. B., Grevemeyer, I., & Rodgers, M. (2018). Tracking Submarine Volcanic Activity at Monowai: Constraints From Long-Range Hydroacoustic Measurements. *Journal of Geophysical Research: Solid Earth*, 123, 7877–7895. doi: 10.1029/2018JB015888
- Metz, D., Watts, A. B., Grevemeyer, I., Rodgers, M., & Paulatto, M. (2016). Ultra-long-range hydroacoustic observations of submarine volcanic activity at Monowai, Kermadec Arc. *Geophysical Research Letters*, 43, 1529–1536. doi: 10.1002/2015GL067259
- Prior, M., Brown, D., Haralabus, G., Stanley, J., & Institute of Acoustics (Great Britain). (2012). Long-term monitoring of ambient noise at CTBTO hydrophone stations. In (pp. 1018—1025). St Albans: Institute Of Acoustics.
- Szuberla, C. A. L., & Olson, J. V. (2004). Uncertainties associated with parameter estimation in atmospheric infrasound arrays. *The Journal of the Acoustical Society of America*, 115, 253–258. doi: 10.1121/1.1635407
- Wessel, P., Luis, J. F., Uieda, L., Scharroo, R., Wobbe, F., Smith, W. H., & Tian, D. (2019). The Generic Mapping Tools Version 6. *Geochemistry, Geophysics, Geosystems*, 20, 5556–5564. doi: 10.1029/2019GC008515
- Wu, W., Zhan, Z., Peng, S., Ni, S., & Callies, J. (2020). Seismic ocean thermometry. *Science*, 369, 1510–1515. doi: 10.1126/science.abb9519